Dipolar Foams in Langmuir Monolayers Dry at Low Bubble Fraction

P. Heinig[†] and Th. M. Fischer*[,‡]

Max Planck Institute of Colloids and Interfaces, Am Mühlenberg 1, D-14476 Golm, Germany, and Department of Chemistry and Biochemistry, The Florida State University, Tallahassee, Florida 32306

Received: November 18, 2002; In Final Form: June 16, 2003

We study the crossover from a hexagonal lattice of circular bubbles to a monodisperse hexagonal foam in two dimensions (2D). A long range $1/r^3$ repulsive interaction (e.g., dipole interaction) is taken into account, and the bubble shape is calculated by numerical solution of the 2D Young−Laplace equation. Unlike short range interaction foams, these foams do not coarsen persistently but reach a local thermodynamic stability at a well-defined bubble size. We find that in (local) thermodynamic equilibrium the bubble shapes depend only on the area fraction of the two phases and not on any material constants; i.e., the bubble shapes of these foams are universal. Experiments with polydisperse dipolar foams in Langmuir monolayers of pentadecanoic acid and myristic acid showed that deformations of the bubbles with respect to the circular shape occur at bubble fractions of ≈70%—in good agreement with the calculated monodisperse foams. This area fraction is much smaller than in short range interaction foams.

1. Introduction

Foams consist of a collection of bubbles surrounded by a continuous phase. If no long range interactions are involved, the total energy of a foam is just the product of the amount of boundary and the interfacial tension (surface tension or line tension). Any reduction in the total amount of interface will reduce the energy. Hence these short range interaction foams are intrinsically unstable, always evolving toward patterns with less interface—they tend to coarsen.[1] In Langmuir monolayers, 2D foams or emulsions are observed,[2−6] exhibiting different natures. An example is shown in Figure 1. Langmuir monolayers are 2D systems of long chain amphiphilic molecules (surfactants) at the air/water interface. They exhibit several phases differing in positional and rotational order, among them 2D liquids and gases. Permanent dipole moments of the surfactants are not screened by the water and result in long range dipole interaction.[7]

The competition between repulsive long range interactions and attractive short range interactions represented by line tension leads to the formation of mesoscopic patterns on a well-defined scale.[8] Unlike in systems with no long range interactions, contributions from repulsive dipolar self-interaction also occur, having the tendency to separate areas of the same phase and to decrease the length scale of the structure. McConnell[9] found that in thermodynamic equilibrium the size of an isolated circular domain is well-defined and determined by the line tension and surface potentials (dipole densities) of the phases. Increasing the radius of the isolated domain above a critical radius leads to a shape transition of the domain to an elongated shape;[10] i.e., an interface line is produced to reduce the dipole interaction energy. Wurlitzer et al.[11] extended the studies of the equilibrium radius to nonisolated domains embedded in a regular lattice. They found that the equilibrium size is increasing with increasing packing density in a characteristic way. A comparison of the thermodynamic stability of this pattern (positive connectivity) with stripe patterns (zero connectivity) or inverted topologies (negative connectivity) by Kwok-On and Vanderbilt[8] showed that foams are in a local minimum of the free energy whereas at intermediate area fractions ($0.28 < \Phi < 0.72$) stripe patterns globally minimize the free energy of the system. Experiments, however, indicate that foam patterns with positive connectivity remain stable with relaxation times exceeding several days.[3]

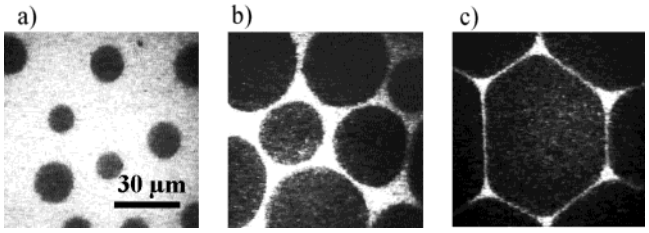

Figure 1. Fluorescence microscopy images of a myristic acid monolayer at (a) 41 Å²/molecule, (b) 46 Å²/molecule, and (c) 51 Å²/molecule showing the crossover from a wet foam toward a dry foam.

In the present paper we focus on the bubble shapes of dipolar 2D foams. One distinguishes between wet and dry foams. Wet foams are solutions of circular bubbles. Increasing the packing density of the bubbles finally leads to a deformation of the bubbles and the foam dries. If no long range interactions are involved, bubbles are deformed if they touch each other. For a monodisperse hexagonal lattice of circular bubbles this is the case at a bubble fraction of 91%,[12] in the case of polydisperse bubbles forming a random Voronoi lattice[13] the critical area fraction $\Phi_c = 84\%$[14] is defined where clusters of touching bubbles percolate through the foam. On further increase of the fraction of the bubble phase, the bubble shapes deviate from circles and end up consisting of facets meeting with an angle of 120° at *Plateau borders*.[15] The shape of the interface is described by the Young−Laplace equation;[16] and the curvature is proportional to the pressure difference across the interface. Short range interaction bubbles consist of regions with constant curvature. The thickness of the facets is in the order of short

* Corresponding author. E-mail: tfischer@chem.fsu.edu.
[†] Max Planck Institute of Colloids and Interfaces, Am Mühlenberg 1, D-14476 Golm, Germany.
[‡] Department of Chemistry and Biochemistry, The Florida State University, Tallahassee, FL 32306.

10.1021/jp0274839 CCC: $25.00 © 2003 American Chemical Society
Published on Web 10/02/2003

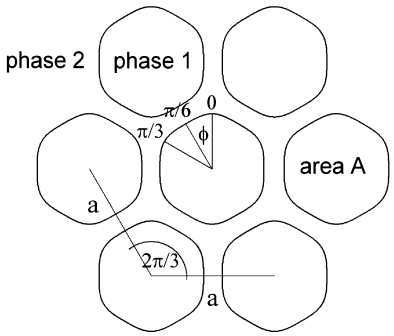

Figure 2. Sketch of a monodisperse foam in hexagonal order. All bubbles (phase 1) have the same shape and area A and form a hexagonal lattice with the lattice constant a. The bubble shape is assumed to have a C_{6v} point group symmetry and is entirely described by its behavior in a polar angle range of $0 < \phi < \pi/6$.

range van der Waals interactions resulting in a disjoining pressure within the facets. The disjoining pressure stabilizes the noncircular bubble shape such that regions of different curvature, i.e., facets and plateau borders, coexist.[15]

In Langmuir monolayers the presence of the long range interaction leads to an electrostatic pressure that depends on the whole foam structure. The Young−Laplace equation holds, here including a term for the dipolar pressure.[17,18] Bubbles do not necessarily consist of circular segments (regions with constant curvature). The shapes of the facets cross over continuously to the shape of the intersection regions determined by long range interactions rather than short range van der Waals interaction. In the present paper we solve the Young−Laplace equation (an integrodifferential equation) by a numerical iteration procedure and study 2D foams with respect to their bubble shapes in size equilibrium. In the experimental part we investigate the deformation of experimental dipolar foams in Langmuir monolayers of pentadecanoic acid and myristic acid.

2. Theory

The total energy of the monolayer associated with a specific pattern is described by the sum of electrostatic dipole (first term) and line tension energies (second term) of all domains:[19,20]

$$F = F_{\mathrm{el}} + F_{\lambda} + F_0 \tag{1}$$

$$= \frac{1}{2}\int \mathrm{d}^2\mathbf{r} \int \mathrm{d}^2\mathbf{r}'\, \mu(\mathbf{r})\, v(\mathbf{r}-\mathbf{r}')\, \mu(\mathbf{r}') + \lambda \int_{\text{phase boundary}} \mathrm{ds} + F_0 \tag{2}$$

where

$$v(\mathbf{r}-\mathbf{r}') = \frac{1}{((\mathbf{r}-\mathbf{r}')^2 + \Delta^2)^{3/2}} \tag{3}$$

describes the dipole interaction potential smoothly screened by the cutoff parameter Δ. The line energy is proportional to the line tension λ between phases 1 and 2 and the total length of the domain boundaries. The material parameter

$$\mu^2(\mathbf{r}) = \begin{cases} 0 & \text{if } \mathbf{r} \in \text{phase 2} \\ \dfrac{\epsilon_0}{4\pi} \dfrac{2\epsilon_{\mathrm{w}}\epsilon_{\mathrm{air}}}{\epsilon_{\mathrm{w}} + \epsilon_{\mathrm{air}}} (V_1 - V_2)^2 & \text{if } \mathbf{r} \in \text{phase 1} \end{cases} \tag{4}$$

characterizes the strength of the dipole interaction energy with respect to the reference phase 2 at the position $\mathbf{r}$. V_1 and V_2 denote the surface potentials of phase 1 and phase 2, where $\epsilon_0 = 8.854$ pN/V^2 is the vacuum permittivity and ϵ_{w} and ϵ_{air} are the relative permittivities of water and air. The cutoff length Δ prevents the integral in (2) from diverging and has been interpreted as intermolecular spacing.[10,19,21] Recent studies by Heinig et al.[22] could show that in a methyl octadecanoate monolayer $\Delta > 0.1$ μm, which suggests that Δ is the range of the short range interactions or the width of the domain borderline. For ferrofluids, which share the same free energy (2) as Langmuir monolayers,[23] Δ is interpreted as the film thickness of the ferrofluid. F_0 is the 2D bulk free energy depending on the areas occupied by the two coexisting phases. The monolayer phase 1 consists of N disjoined domains and the free energy equation (2) describes the energy of the N domains.

At local thermodynamic equilibrium the curvature $\kappa(\mathbf{r})$ of a domain at position $\mathbf{r}$ at the boundary is proportional to the pressure difference across the interface (2D Young−Laplace equation[10,17,18,22]):

$$\lambda\kappa(\mathbf{r}) = p + p_{\mathrm{el}}(\mathbf{r}) \tag{5}$$

with the electrostatic pressure

$$p_{\mathrm{el}}(\mathbf{r}) = \int \mathrm{d}^2\mathbf{r}'\, \mu(\mathbf{r})\, v(\mathbf{r}-\mathbf{r}')\, \mu(\mathbf{r}') \tag{6}$$

Because of a shape invariant scaling transformation shown in refs 10, 17, 18, and 22, the shape of a domain with the area A only depends on the geometry of the surroundings and on the dimensionless interaction parameter

$$\tilde{\lambda}^* = \frac{\lambda}{\mu^2} - \ln\frac{\sqrt{A}}{\Delta} \tag{7}$$

Let us assume a monodisperse periodic hexagonal foam (Figure 2). Then the structure of the surroundings is determined by the gas fraction of the phases $\Phi = A/a^2 \sin(\pi/3)$ (a the lattice constant) and the shape $\mathbf{r}$ is a function of Φ, A, and $\tilde{\lambda}^*$:

$$\mathbf{r} = \sqrt{A}\tilde{\mathbf{r}}(\Phi, \tilde{\lambda}^*) \tag{8}$$

where the dimensionless $\tilde{\mathbf{r}}$ stands for a shape of unit area.

As mentioned in the Introduction, Langmuir monolayer foams reach a local thermodynamic equilibrium.[9,11] At this equilibrium the free energy (1) is a minimum with respect to the size of a domain:

$$\left.\frac{\partial F}{\partial A}\right|_{\Phi,\Delta,\lambda,\mu^2} = 0 \tag{9}$$

Making use of the shape invariant scaling transformation, eq 9 can be rewritten as a minimization of a function $\tilde{f}$ involving the parameters A, Δ, λ, and μ only in the form of the interaction parameter $\tilde{\lambda}^*$ (Appendix A). The minimization with respect to the interaction parameter

$$\frac{\partial}{\partial\tilde{\lambda}^*} \mathrm{e}^{\tilde{\lambda}^*} \tilde{f}(\tilde{\lambda}^*, \Phi) = 0 \tag{10}$$

then determines $\tilde{\lambda}^*$ as a function of Φ.

Inserting $\tilde{\lambda}^*(\Phi)$ into eq 8 yields the unit equilibrium shape

$$\tilde{\mathbf{r}}_{\mathrm{eq}} = \tilde{\mathbf{r}}_{\mathrm{eq}}(\Phi) \tag{11}$$

So the shape $\tilde{\mathbf{r}}_{\mathrm{eq}}$ of the bubbles in a periodic dipolar foam is universal and depends only on the area fraction Φ and not on the material constants (λ, Δ, or μ).

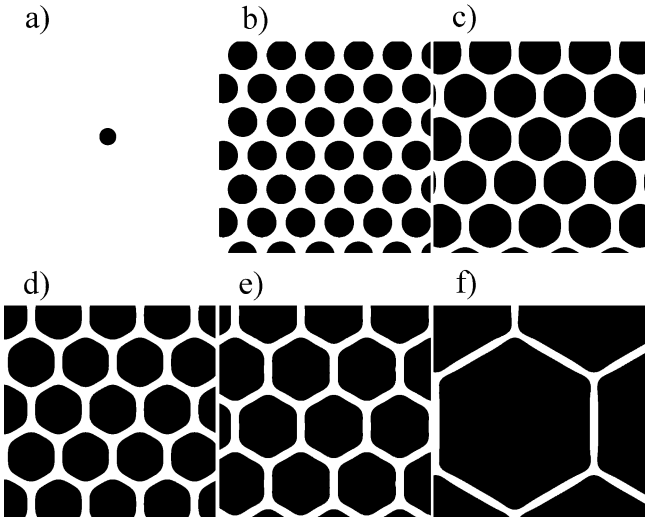

Figure 3. Simulated foams for area fractions (a) $\Phi = 0$, (b) $\Phi = 0.5$, (c) $\Phi = 0.65$, (d) $\Phi = 0.683$, (e) $\Phi = 0.74$, and (f) $\Phi = 0.9$. Upon increasing Φ, the bubble size increases. The foam structure changes from an emulsion of circular bubbles (a) and (b) via (c), (d), and (e) to a dry foam with almost hexagonal shape (f).

For the size one finds (Appendix A)

$$\sqrt{A} = \sqrt{A_0}\mathrm{e}^{Y(\Phi)} \tag{12}$$

where $Y(\Phi)$ is a universal size function and A_0 is the equilibrium size of an isolated domain[9]

$$\sqrt{A_0} = \Delta\frac{\sqrt{\pi}e^2}{8}\mathrm{e}^{\lambda/\mu^2} \qquad \left(\equiv\tilde{\lambda}^{*0} = \ln\frac{8}{\sqrt{\pi}e^2}\right) \tag{13}$$

The size A_0 depends on the materials parameters. At vanishing dipole interaction, $\mu = 0$, it diverges.

3. Numerics

The aim is to numerically find the equilibrium foam structure (bubble size and shape) for a given area fraction Φ of the two phases. The infinite regular lattice was approximated by one central bubble and 20 layers of neighbors, i.e., 1260 surrounding bubbles, in hexagonal order with the lattice constant a (Figure 2). The large number of bubbles provides a high accuracy (error $< 1\%$) of the simulated shapes.

The Young−Laplace equation is solved by assuming all bubbles of the foam have the same shape. The shape for a given Φ and $\tilde{\lambda}^*$ has been calculated using the procedure described in Appendix B, a slightly modified version from the one used in ref 22. The free energy is minimized using the modified dimensionless free energy (A4) and solving the minimum condition (10) as described in Appendix B.

In Figure 3 simulated foams and their respective emulsions are shown. In (a) at $\Phi \approx 0$ there is one isolated domain. Its size A_0 is given by eq 13 found by McConnell.[9] In (b) the amount of the black phase is 50% and the domains are almost circular. A further increasing of the area fraction to (c) (65%) leads to increase of equilibrium size and a deformation of the bubbles. In (d) (68.3%) and (e) (74%) foams are formed and at high Φ (f) (90%) dry foams occur with almost perfect hexagonal bubble shape.

Bubble Size. In Figure 4 the relative size $\sqrt{A/A_0}$ is plotted as a function of the area fraction Φ (black dots). At lower surface fractions, $\Phi \lesssim 0.85$, the relative bubble size is well described by a model considering circular domains[11] (gray dots)

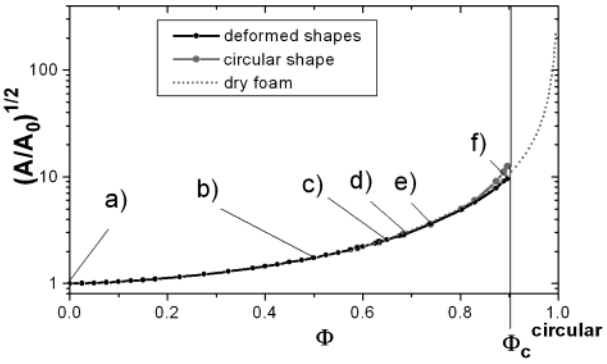

Figure 4. Relative bubble areas $\sqrt{A/A_0} = \mathrm{e}^{Y(\Phi)}$ versus the area fraction Φ at (local) thermodynamic equilibrium of deformed bubbles (black dots), circular bubbles[11] (gray dots) and a dry hexagonal foam of noninteracting facets (line).

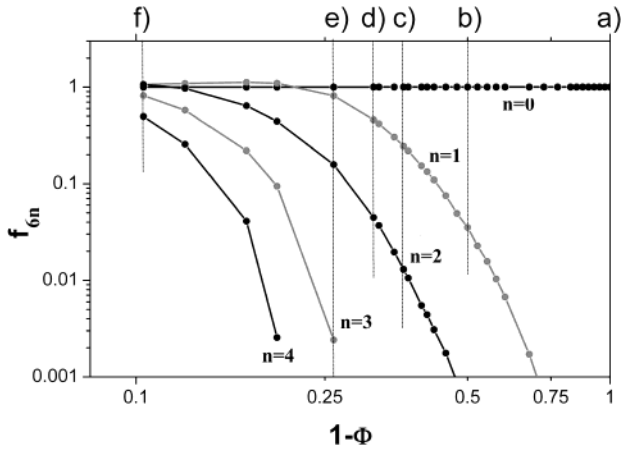

Figure 5. Bubble shape parameters f_{6n} versus area fraction. The shape parameters f_{6n} (16) switch from 0 to 1 as the shape changes from circular toward hexagonal upon increasing the area fraction Φ.

whereas at higher surface fractions, $\Phi \gtrsim 0.85$, the approximation of the foam by noninteracting liquid facets (line) fits quite well

$$\frac{A_{\text{dry foam}}}{A_0} = \frac{8}{e^2}\sqrt{\frac{2\sqrt{3}}{\pi}}\sqrt{\frac{\Phi}{1-\Phi}} \tag{14}$$

The bubble size of a dry foam diverges at $\Phi = 1$.

Bubble Shape. Figure 5 shows the results of the shape analysis. The numerical equilibrium shapes are expressed as a function of their arc length s. We performed a change of coordinate system from the arc length toward a polar coordinate system, $\tilde{\mathbf{r}}(s) \rightarrow \tilde{\mathbf{r}}(\phi)$ and performed a Fourier expansion, which due to symmetry reasons reads

$$\tilde{\mathbf{r}}(\phi) = \frac{c_0}{2} + \sum_{n=1}^{\infty} c_{6n}\cos(6n\phi) \tag{15}$$

The origin is set to the center of the bubble and $\mathbf{r}(\phi = 0)$ is pointing to an edge. We express the Fourier coefficients c_{6n} as

$$c_{6n} = c_{6n}^{\text{hex}} f_{6n}(\Phi) \tag{16}$$

with c_{6n}^{hex} the Fourier coefficients of the unit hexagon[24] and the $f_{6n}(\Phi)$ area fraction dependent coefficients describing the deviation of the shape from a hexagon. The coefficient f_0 is approximately 1 for all values of Φ. For $n > 0$, $f_{6n} = 0$ corresponds to a circle and $f_{6n} = 1$ to a hexagon. In Figure 5

we plot the values of f_{6n} versus the area fraction. The crossover from circular shapes to hexagonal shapes happens between 65% and 80% area fraction, where $0.3 < f_6 \leq 1$.

4. Experimental Foams

Myristic acid and pentadecanoic acid from Sigma were spread at room temperature (≈20 °C) from a chloroform solution on pure water subphase (Milli Q). The patterns were observed using fluorescence microscopy,[2] with 1 mol % fluorescence dye (NBD-HDA, Molecular Probes) added to the chloroform solution. Fluorescence microscopy is the technique of choice because 2D liquids and 2D gases are well distinguishable. The fluorescence dye might have an effect on the interaction parameters. For the experiments, however, the interaction parameters are not needed to be known in detail (see also argument in ref 3). The monolayer was spread to an area of $A_{\mathrm{mol}} \approx 35$ Å^2 per molecule, where no gaseous phase occurs. Slow isothermal expansion (<0.2 Å^2 per molecule and minute) leads to the formation of small gas bubbles at $A_{\mathrm{mol}} \approx 40$ Å^2 per molecule (Figure 1a), deformed bubbles at $A_{\mathrm{mol}} \approx 45$ Å^2 per molecule (Figure 1b) and dry foams at areas larger than $A_{\mathrm{mol}} \approx 50$ Å^2 per molecule. The images were recorded and digitized for further evaluation.

The observed foams consist of polydisperse bubbles in irregular order (Figure 1a−c). Deformations are in general not 6-fold symmetric and a direct comparison of the shape coefficients f_{6n} (16) is not possible. We decided to take the mean square deviation from a circle

$$\sigma^2 = \frac{\langle(\mathbf{r} - \mathbf{r}_c)^2\rangle - \langle|\mathbf{r} - \mathbf{r}_c|\rangle^2}{\langle|\mathbf{r} - \mathbf{r}_c|\rangle^2} \tag{17}$$

as a measure for the deformation of the bubbles, where the average of B over the boundary of the domain is defined as

$$\langle B\rangle = \frac{\int B(\mathbf{r} - \mathbf{r}_c)\cdot\mathbf{n}\, \mathrm{d}s}{\int (\mathbf{r} - \mathbf{r}_c)\cdot\mathbf{n}\, \mathrm{d}s} \tag{18}$$

and $\mathbf{r}_c = \langle\mathbf{r}\rangle$. This choice of weighted average coincides with the definition of an area average

$$\langle B\rangle = \frac{\int B\, \mathrm{d}A}{A} \tag{19}$$

if B is continued from the domain boundary to the interior such that $\int \nabla B\cdot(\mathbf{r} - \mathbf{r}_c)\, \mathrm{d}A = 0$.

The deformation parameters σ^2 were determined for 150 experimental bubbles at different area fractions Φ. The area fraction Φ was measured in the direct environment of the investigated bubble by a histogram of the fluorescence image. The result is plotted in Figure 6. An experimental trend is obtained by averaging the σ^2 of domains falling into the same intervals of widths 0.1 of the area fraction Φ. The error bars in σ^2 are due to statistical fluctuations between different domains, whereas the errors in Φ arise due to a limited field of view and due to a biased choice of images associated with this (Only images where domains lay entirely within the field of view can be analyzed.)

Values of σ^2 measured in experiments are larger than the theoretical predictions. At low area fractions $\Phi < 0.6$, this deviation is an artifact arising from pixelized boundaries of the domains on the scale of the resolution of the images. At larger area fractions $\Phi > 0.6$, where deformations are larger, it is a real effect due to the fluctuations in shape between individual domains. These shape fluctuations are suppressed in the monodisperse periodic foam simulations. Large domains in the experiments often exhibit a 2-fold deformation, which can be much larger than the deformation of a circle toward an ideal hexagon. With respect to most characteristics of the monodisperse hexagonal foam, experiment does not match the theory. However, the crossover from a wet foam (circular droplets) toward a dry foam (distorted or faceted droplets) in the experiments occurs at the same area fraction $\Phi_c \approx 0.7$ as predicted for the monodisperse hexagonal foam. This crossover happens well below the critical area fraction of closed packed monodisperse circular domains $\Phi_c = 0.91$[12] and of polydisperse bubbles $\Phi_c = 0.84$ simulated using a random Voronoi lattice.[14] In contrast to short range interaction foams, where the critical packing fraction is a purely geometrical effect, the crossover toward deformed domains in Langmuir monolayers arises due to the long range nature of the interactions.

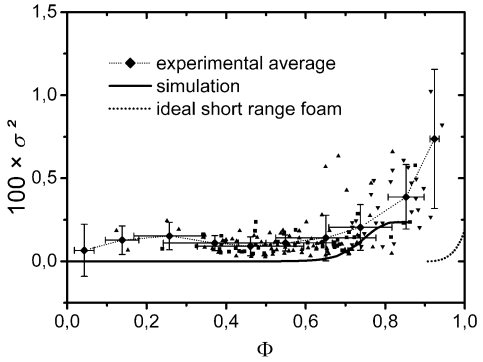

Figure 6. Experimental (▲ and ▼, myristic acid; ■, pentadecanoic acid; ◆, average of the experiments) and theoretical (periodic hexagonal foam) values of the deformation parameter σ^2 (eq 17) versus the area fraction Φ. The experimental averages were calculated over an interval of $[\Phi - 0.05, \Phi + 0.05)$ with the standard deviations plotted as error bars.

5. Discussion

Due to long range dipole interactions, foams in Langmuir monolayers do not coarsen persistently but reach a local thermodynamic equilibrium on a well-defined length scale. The size of the bubbles depends on the materials parameters (dipole density, line tension) and diverges as the dipole density approaches zero. Only in the limit of vanishing long range interaction are the foams intrinsically unstable: the larger structure always has less energy. It has to be mentioned that Berge et al.[3] observed a coarsening in Langmuir foams. The presented images of Berge et al., however, are not at constant gas fraction and are consistent also with the interpretation that the size is determined by the gas fraction rather than the relaxation time.[25] The formation of mesoscopic patterns in local thermodynamic equilibrium in Langmuir monolayers is well accepted.[8,9,11]

The bubble shapes of a monodisperse hexagonal dipolar 2D foam in equilibrium are universal. They depend only on the area fraction of the phases and not on material constants. The size of the bubbles is described by a universal size function in units of the equilibrium radius of an isolated domain A_0 and diverges as the bubble fraction approaches $\Phi = 1$. In fact, A_0 is the only materials parameter necessary for the description of monodisperse hexangonal dipolar 2D foams. It is a function of the dipole densities, line tension and cutoff length. The crossover from a wet to a dry monodisperse hexagonal dipolar 2D foam

occurs at a bubble fraction of $\Phi \approx 0.7$, which is significantly lower than the critical area fraction $\Phi_c = 0.91$ of a monodisperse short range interaction 2D foam in hexagonal order.[12]

Experimental foams observed in Langmuir monolayers are polydisperse foams. However, the transition point from a wet to dry foam, i.e., the area fraction at which bubbles are significantly deformed, agrees with the calculated monodisperse foam in hexagonal order. We suspect that effects of nonideality just compensate. The measured transition fraction of $\Phi \approx 0.7$ is lower than in polydisperse short range interaction 2D foams $\Phi_c = 0.84$ estimated by Bolton and Weaire[14] by computer simulations using a random Voronoi lattice.[13]

The presented theory could be applied also to foams observed in ferrofluids.[26]

Appendix A: Energy Minimization

In this appendix the shape invariant minimization of the dipolar foam with respect to the size of the bubbles (10) is derived. Because $(\partial/\partial A)AN|_\Phi = (\partial/\partial A)A_{total}\Phi|_\Phi = 0$, the equilibrium condition (9) corresponds to minimizing the function f

$$\left.\frac{\partial f}{\partial A}\right|_{\Phi,\Delta,\lambda,\mu^2} = 0 \qquad \text{where} \qquad f = \frac{F - F_0}{AN} - \frac{\mu^2 \pi}{\Delta} \tag{A1}$$

It has been shown by de Koker and McConnell[10] that f is invariant to shape invariant scaling transformation and so, similar to $\mathbf{r}$, it can be expressed in the form

$$f(\lambda,\mu^2,\Delta,A,\Phi) = \frac{\mu^2}{\sqrt{A}}\tilde{f}(\tilde{\lambda}^*,\Phi) \tag{A2}$$

with the dimensionless $\tilde{f}$.

With $\partial\tilde{\lambda}^*/\partial A = -1/(2A)$ one finds (10), which determines a relation between the interaction parameter $\tilde{\lambda}^*$ and the area fraction Φ. We express the solution of eq 10 in the form

$$\tilde{\lambda}^* = \tilde{\lambda}_0^* - Y(\Phi) \tag{A3}$$

with $\tilde{\lambda}_0^*$ defined in (13). Using the definition of $\tilde{\lambda}^*$ (7) yields eq 12.

For numerical minimization we used the expression

$$\tilde{f} = -\frac{1}{2} \oint_{\substack{\text{central domain}\\ \text{boundary}}} \oint_{\substack{\text{all domain}\\ \text{boundaries}}} \frac{d\tilde{s}\cdot d\tilde{s}'}{\sqrt{(\tilde{\mathbf{r}} - \tilde{\mathbf{r}}')^2 + \Delta^2/A}} + (\lambda/\mu^2 - 1) \oint_{\substack{\text{central domain}\\ \text{boundary}}} d\tilde{s} \tag{A4}$$

where the integration over s (s') is performed along the interface of the central domain (all domains). We fixed without loss of generality $\sqrt{A}/\Delta = 100$. A Newton procedure has been used to solve eq 10. The accuracy of the calculated interaction parameter $\tilde{\lambda}^*$ is about ± 0.01.

Appendix B: Numerical Solution of the Young-Laplace-equation

Here we give a brief description of the numerics used to calculate the bubble shape. In contrast to the procedure described in ref 22 a C_{6v} symmetry is included in the Young−Laplace equation. The shape of the bubble is described by $\mathbf{r}(s)$, where s is the arc length with values between 0 and the perimeter P. It is chosen in a way such that $\mathbf{r}(0)$ points to an edge of the bubble.

Further we use a damped iteration method instead of normal iteration:

$$\kappa_{n+1}(s) = (1 - q)\kappa_n(s) + q\left(\frac{2\pi}{P} - \frac{\mu^2}{\lambda}\delta I_n(s)\right) \tag{B1}$$

with

$$\delta I_n(s) = I_n(s) - \frac{12}{P}\int_0^{P/12} ds'\, I_n(s') \tag{B2}$$

with

$$I_n(s) = -12 \sum_{\text{i=all bubbles}} \int_0^{P/12} ds' \frac{\mathbf{n'}_n\cdot(\mathbf{r}_n - \mathbf{r'}_n)}{(\mathbf{r}_n - \mathbf{r'}_n)^2\sqrt{(\mathbf{r}_n - \mathbf{r'}_n)^2 + \Delta^2}} \tag{B3}$$

where n denotes the iteration step and $0 < q \leq 1$ is the damping factor. The choice of $q = 0.5$ showed best results.

The curvature $\kappa_{n+1}(s)$ determines the shape $\mathbf{r}_{n+1}(s)$ and the interaction integral $\delta I_{n+1}(s)$ also described in ref 22. As in ref 22 the perimeter P is replaced by the bubble area $\tilde{A}$ by application of a regula falsi iteration. The procedure is repeated until the bubble area $\tilde{A}$ equals 1 with sufficient precision. As a result we obtain the bubble shape $\tilde{\boldsymbol{r}}(s)$ as function of the dimensionless parameters (λ/μ^2, $\Delta/\sqrt{A}$, Φ), where $\sqrt{A}/\Delta = 100$ is kept fixed.

The arc segment is discretized by 100 sampling points, i.e., 1200 sampling points for the whole domain. So Δ is larger than the numerical step width and smaller than the curvature radius ($ds < \Delta < \kappa_{min}^{-1}$), a necessary condition for the validity of the scaling law and eq 7.

References and Notes

(1) Glazier, J. A.; Weaire, D. *J. Phys: Condensed Matter* **1992**, *4*, 1867.

(2) Lösche, M.; Sackmann, E.; Möhwald, H. *Ber. Bunsen-Ges., Phys. Chem.* **1983**, *87*, 848.

(3) Berge, B.; Simon, A. J.; Libchaber, A. *Phys. Rev. A* **1990**, *41*, 6893.

(4) Stine, K. J.; Bono, M. F.; Kretzer, J. S. *J. Colloid Interface Sci.* **1994**, *162*, 320.

(5) Dennin, M.; Knobler, C. M. *Phys. Rev. Lett.* **1996**, *78*, 2485.

(6) Mann, E. K.; Primak, V. *Phys. Rev. Lett.* **1999**, *83*, 5397.

(7) Demchak, R. J.; Fort, T., Jr. *J. Colloid Interface Sci.* **1973**, *46*, 191.

(8) Kwok-On, Ng, Vanderbilt, D. *Phys. Rev. B* **1995**, *52*, 2177.

(9) McConnell, H. M. *Proc. Natl. Acad. Sci. U.S.A.* **1989**, *86*, 3452.

(10) de Koker, R.; McConnell, H. M. *J. Phys. Chem.* **1993**, *97*, 13419.

(11) Wurlitzer, S.; Schmiedel, H.; Fischer, Th. M. *J. Chem. Phys.* **2002**, *116*, 10877.

(12) Princen, H. M. *J. Colloid Interface Sci.* **1979**, *71*, 55.

(13) Kermode, J. P.; Weaire, D. *Comput. Phys. Commun.* **1990**, *60*, 75.

(14) Bolton, F.; Weaire, D. *Philos. Mag. B* **1992**, *65*, 473.

(15) Hutzler, S.; Weaire, D. *The Physics of Foams*; Oxford University Press: Oxford, U.K., 1999.

(16) Graner, F.; Jiang, Y.; Flament, C. *Phys. Rev. E* **2000**, *63*, 011402.

(17) Riviére, S.; Henon, S.; Meunier, J.; Albrecht, G.; Boissonade, M. M.; Baszkin, A. *Phys. Rev. Lett.* **1995**, *75*, 2506.

(18) Heinig, P.; Steffen, P.; Wurlitzer, S.; Fischer, Th. M. *Langmuir* **2001**, *17*, 6633.

(19) McConnell, H. M. *Annu. Rev. Phys. Chem.* **1991**, *42*, 171.

(20) Seul, M.; Andelman, D. *Science* **1995**, *267*, 476.

(21) Hurley, M. M.; Singer, S. J. *J. Phys. Chem.* **1992**, *96*, 1938.

(22) Heinig, P.; Wurlitzer, S.; John, Th.; Fischer, Th. M. *J. Phys. Chem.* **2002**, *106*, 11951.

(23) Elias, F.; Flament, C.; Bacri, J.-C.; Neveu , S. *J. Phys. I Fr*. **1997**, *7*, 711.

(24) The Fourier coefficients of the unit hexagon are $c_{6n}^{\mathrm{hex}} = 2^{-1/2}3^{3/4}\pi^{-1}[\ln 3 + \Psi(n + {}^1/_2) - \Psi(3n + {}^1/_2)]$, where $\Psi(z) = \mathrm{d/dz}\ \ln(\Gamma(z))$ is the digamma function. The values of the first coefficients are $c_0^{\mathrm{hex}} = 0.564$, $c_6^{\mathrm{hex}} = 1.64 \times 10^{-2}$, $c_{12}^{\mathrm{hex}} = 4.54 \times 10^{-3}$, ...

(25) Data taken from Figure 3 in ref 3: The bubble area in Figure 3e ($\Phi \approx 0.67$) is approximately 4 times as large as that in Figure 3c ($\Phi \approx 0.4$). Assuming size equilibrium (Figure 4 of the present paper and ref 11), the predicted area is $A(\Phi{=}0.67) \approx 3.7A(\Phi{=}0.4)$.

(26) Elias, F.; Flament, C.; Bacri, J.-C.; Cardoso, O.; Graner, F. *Phys. Rev. E* **1997**, *56*, 3310.